ELSEVIER

Materials Science and Engineering A327 (2002) 89–93

MATERIALS SCIENCE & ENGINEERING A

www.elsevier.com/locate/msea

Microstructural characterization of Haynes® 242™ alloy

M.K. Miller [a,*], I.M. Anderson [a], L.M. Pike [b], D.L. Klarstrom [b]

[a] *Microscopy and Microanalytical Sciences Group, Metals and Ceramics Division, Oak Ridge National Laboratory, P.O. Box 2008, Oak Ridge, TN 37831-6136, USA*

[b] *Haynes International Inc., 1020 W. Park Avenue, Kokomo, IN 46904-9013, USA*

Abstract

A microstructural characterization has been performed on a HAYNES 242 nickel-molybdenum-chromium superalloy. Molybdenum was found to partition to the lenticular $Ni_2(Mo,Cr)$ precipitates whereas iron, aluminum, silicon, manganese and nickel were found to partition to the γ matrix. Chromium was not found to partition significantly between the phases. Atom probe tomography and energy-filtered transmission electron microscopy core-loss images revealed boron, molybdenum, chromium, phosphorus and carbon segregation to the grain boundaries. Despite the size of the precipitates being larger after a two-step heat treatment of 16 h at 704 °C + 16 h at 650 °C compared to a one-step heat treatment of 48 h at 650 °C, no significant differences were found in the mechanical properties or the compositions of the phases. Published by Elsevier Science B.V.

Keywords: Superalloy; Haynes 242; Atom probe tomography; Grain boundary segregation; Partitioning

1. Introduction

HAYNES 242 alloy is an age-hardenable nickel-molybdenum-chromium superalloy that derives its good mechanical properties from a fine dispersion of metastable $Ni_2(Mo,Cr)$ ordered body centered orthorhombic (Pt_2Mo-type) domains/precipitates in a face centered cubic γ matrix [1–3]. Previous studies have revealed that the matrix retains a high temperature short range ordered (SRO) structure after water quenching from the solution treatment [4]. This superalloy exhibits low thermal expansion characteristics, good thermal stability, good oxidation resistance up to 815 °C, good low-cycle fatigue properties and resistance to high temperature fluorine and fluoride environments. HAYNES 242 alloy is typically used for gas turbine engine seal and containment rings, duct segments, casings, fasteners, rocket nozzles and pumps.

The aim of this project was to compare the microstructures and mechanical properties of 242 alloy after a one-step heat treatment and after a shorter and therefore more cost effective two-step heat treatment [5].

2. Experimental

The composition of the commercial 242 superalloy used in this investigation was: Ni- 16.4at% Mo, 9.3% Cr, 1.3% Fe, 0.45% Al, 0.37% Mn, 0.14% Si, 0.018% B, 0.027% C and <0.01% P. The superalloy was given a standard anneal of 0.5 h at 1066 °C and water quenched to room temperature prior to a two-step heat treatment of 16 h at 704 °C + 16 h at 650 °C or a one-step heat treatment of 48 h at 650 °C. The superalloy was air cooled to room temperature after each stage.

The microstructural characterizations were performed with the ORNL energy-compensated optical position-sensitive atom probe [6], a Philips CM30 transmission electron microscope (TEM) equipped with a Gatan Imaging Filter (GIF), and a Philips XL30 scanning electron microscope (SEM). The grain size was determined with the use of backscattered electron (BSE) imaging in the SEM, and the structure of the precipitates was analyzed by convergent beam electron diffraction (CBED) in the TEM. Elemental 'jump ratio' images were formed from pairs of energy-filtered TEM core-loss images, by dividing an image acquired with electron energies greater than a characteristic edge of the relevant element by the corresponding image acquired with electron energies immediately preceding the

* Corresponding author. Tel.: +1-865-574-4719; fax: +1-865-241-3650.

E-mail address: millermk@ornl.gov (M.K. Miller).

0921-5093/02/$ - see front matter. Published by Elsevier Science B.V.
PII: S0921-5093(01)01882-2

edge onset. Energy-filtered jump ratio images were used to qualitatively assess the partitioning of elements between the precipitates and the matrix, and the segregation at grain boundaries. Atom probe tomography (APT) was used to quantify the partitioning and segregation behavior.

3. Experimental results

3.1. Mechanical properties

The mechanical properties of these materials at 650 °C were determined and the results are summarized in Table 1. Although these two heat treatments produced materials with similar mechanical properties, the yield strength and ultimate tensile strength were significantly lower and the elongation and reduction in area were significantly higher after the first stage (16 h at 704 °C) of the two-stage heat treatment. Therefore, the second low temperature stage of the heat treatment (16 h at 650 °C) is an important step in producing the desired mechanical properties. At 650°C, the fracture mode started as intergranular and then changed to shear. No difference in the fracture mode was observed between the two heat treatments.

3.2. Intragranular microstructure

Convergent beam electron diffraction analysis established that the precipitates had an ordered Pt_2Mo-type crystal structure, in agreement with previous studies [7]. Energy-filtered jump ratio images acquired in the vicinity of the Mo M-edge indicate that the $Ni_2(Mo,Cr)$ precipitates are ellipsoidal disks with an aspect ratio of approximately 8:5:1 in the major, intermediate and minor dimensions, as shown in Fig. 1. The major dimension of the precipitates was found to be significantly larger, ~150 nm, after the two-step heat treatment compared to ~25 nm after the one-step heat treatment as shown in Figs. 1a and 1b, respectively. Similar images acquired from an alloy subjected only to the first step of the two-step heat treatment showed that the precipitates were of similar size to those shown in Fig. 1a, indicating that there was little discernable change in the size of the precipitates during the second step of the two-step heat treatment.

Table 1
Summary of the mechanical properties of Haynes 242 as a function of the heat treatment

Heat treatment	Yield strength MPa	Ultimate tensile strength, MPa	Elongation, %	Reduction in area, %
48 h at 650 °C	622	1022	24.6	32.1
16 h at 704 °C	435	916	36.1	39.7
16 h at 704 °C + 16 h at 650 °C	652	1015	23.0	27.6

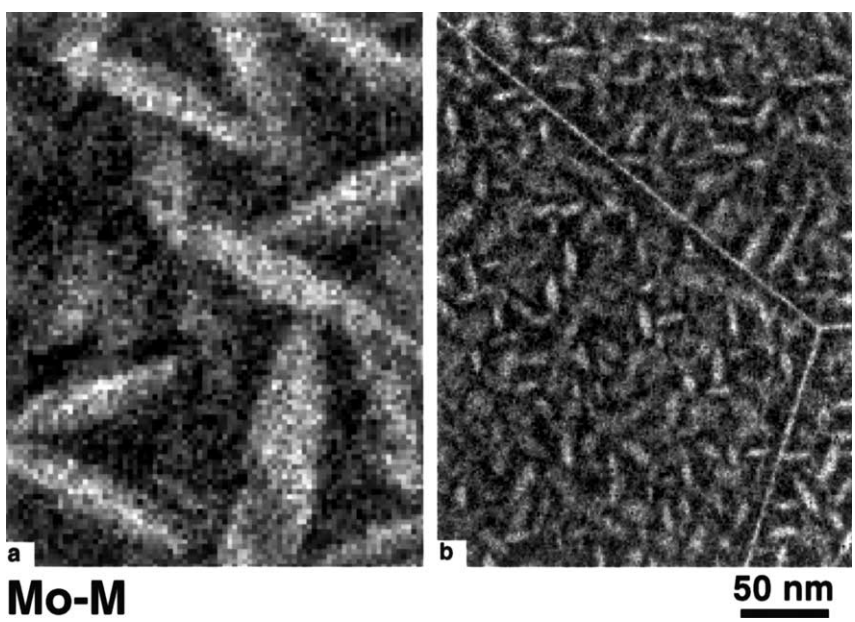

Fig. 1. Mo-M jump ratio energy filtered images of the microstructure: (a) two-step heat treatment of 16 h at 704 °C + 16 h at 650 °C; and (b) one-step heat treatment of 48 h at 650 °C.

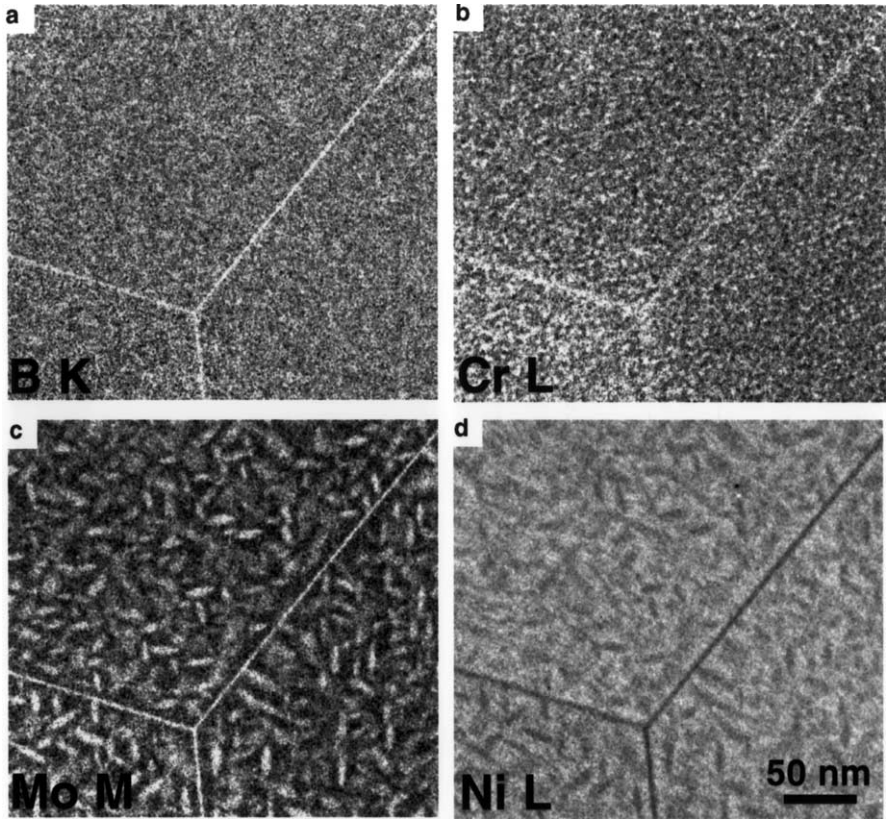

Fig. 2. Energy-filtered jump ratio images in the vicinity of a triple grain junction for the two-step heat treatment: (a) B K; (b) Cr L; (c) Mo M; and (d) Ni L edges.

A series of energy-filtered images showing the partitioning of nickel, molybdenum, chromium and boron in the vicinity of a triple grain junction is shown in Fig. 2. These images show qualitatively that nickel partitions to the γ matrix, molybdenum partitions to the precipitates and that neither chromium nor boron partition substantially between the two phases. The elemental partitioning between the γ matrix and the $Ni_2(Mo,Cr)$ precipitates was determined quantitatively by atom probe tomography. The results are summarized graphically in Fig. 3. The partitioning of the major elements was in agreement with the energy-filtered imaging results. In addition, the trace elements iron, aluminum, silicon and manganese were found to partition to the γ matrix. The partitioning behavior for most elements was similar between the heat treatments. However, the molybdenum level in the γ matrix after the first stage of the two-stage heat treatment was significantly higher than after the second stage or after the one-step heat treatments. This decrease in molybdenum level suggests an increase in the volume fraction of the precipitates. Composition profiles across the precipitate-matrix interface are shown in Fig. 4. Evidence of chromium enrichment at the interface is apparent after the two-step heat treatment.

3.3. Grain boundaries

The grain sizes of these materials were ~ 40 μm, independent of the heat treatment, as measured from BSE images in the SEM. Field ion micrographs of a grain boundary in the two-step heat treatment revealed bright spot decoration indicative of solute segregation, as shown in Fig. 5. Energy-filtered imaging revealed that there was no significant disruption of the precipitate morphology at the grain boundaries. Therefore, there were segments of the grain boundary that exhib-

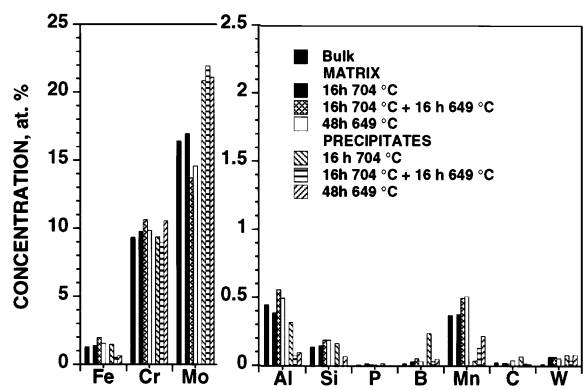

Fig. 3. Partitioning behavior of the alloying elements as determined from atom probe tomography.

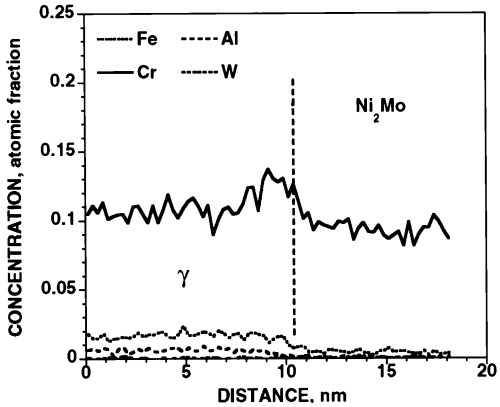

Fig. 4. Composition profiles across the ordered $Ni_2(Mo,Cr)$ precipitate-matrix interface.

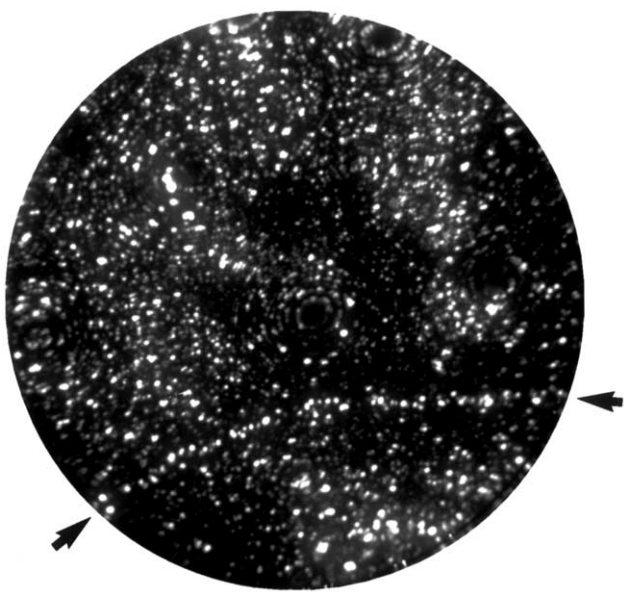

Fig. 5. Field ion micrograph of a grain boundary in the two-step heat treatment showing bright spot decoration indicative of solute segregation.

ited precipitate-precipitate, precipitate-matrix and matrix–matrix interfaces, as demonstrated in an energy-filtered jump ratio images in Fig. 2. These images indicate the segregation of boron and molybdenum, and the depletion of nickel, at the grain boundaries. The chromium map, which exhibits poorer signal-to-noise, also shows a weak enhancement of signal at the boundary. However, the interpretation of this signal is complicated by the close proximity of the oxygen K edge to the chromium L edge. An atom map of a portion of a grain boundary that includes precipitate-matrix and matrix–matrix segments is shown in Fig. 6. The area of slightly higher molybdenum content indicates the position of the precipitate. From a selected volume analysis of a matrix-matrix region of the boundary, the Gibbsian interfacial excesses were determined and the results are given in Table 2. Boron, phosphorus, carbon and molybdenum were found to be significantly enriched and a small enrichment of tungsten was observed. The results indicated that silicon was essentially randomly distributed. The levels of iron, chromium, nickel and aluminum were found to be depleted at the grain boundary. Composition profiles across precipitate-matrix and matrix–matrix segments of this grain boundary are shown in Fig. 7. Segregation of boron, phosphorus and molybdenum to the boundary is clearly revealed. The full width at half maximum of the boron segregation was ~ 4 nm. However, a ~ 1-nm-wide depletion in the atom density due to trajectory aberrations in the vicinity of the grain boundary was observed in the atom map. Therefore, this value is an overestimate of the width of the segregation. A small enrichment of chromium was also evident at the precipitate-matrix interface.

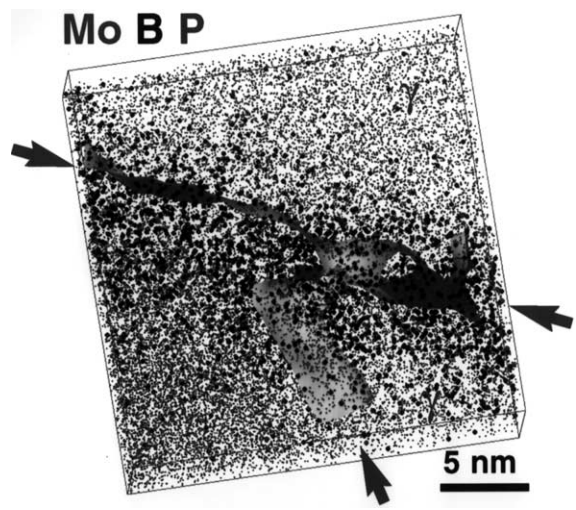

Fig. 6. A 3-dimensional atom map of a portion of a grain boundary that includes precipitate-matrix and matrix–matrix segments. The $\sim 17\%$ Mo isoconcentration surface indicates the positions of the precipitate-matrix interface and the grain boundary. Both boron and phosphorus segregation to the boundary are clearly revealed.

Table 2
Gibbsian interfacial excess of the two-step heat treated material as determined from selected volume analysis in the three-dimensional atom probe

Element	Gibbsian interfacial excess, atoms m^{-2}
Boron	6.5×10^{18}
Phosphorus	5.9×10^{17}
Carbon	1.3×10^{17}
Molybdenum	1.7×10^{19}
Tungsten	4.7×10^{16}
Silicon	1.9×10^{16}

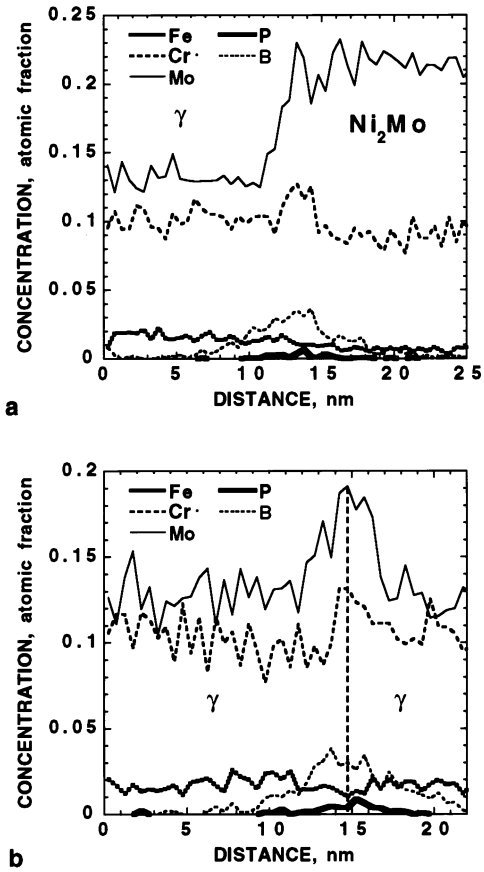

Fig. 7. Composition profiles perpendicular to: (a) the precipitate-matrix interface at the grain boundary; and (b) the matrix-matrix grain boundary shown in Fig. 6.

4. Discussion

The yield strength, ultimate tensile strength, elongation and reduction in area of the materials after the one-step (48 h at 650 °C) and two-step (16 h at 704 °C + 16 h at 650 °C) heat treatment were similar. In addition, the grain sizes and compositions of the γ matrix and the $Ni_2(Mo,Cr)$ precipitates were comparable. Since the compositions of the two phases were similar after these heat treatments, the volume fractions of the phases must also be similar due to the constraints of the lever rule and assuming that the compositions of the phases had attained their equilibrium values. However, the size of the precipitates was significantly larger and consequently, the amount of interfacial area was smaller, after the two-step heat treatment compared to a one-step heat treatment. These differences did not appear to influence the mechanical properties.

The yield and ultimate tensile strengths of the material after the first stage of the two-step heat treatment were significantly lower than after the second stage and the elongation and reduction in area were higher. These variations are probably due to the observed small differences in compositions and volume fraction of the phases and also possibly the degree of order of the $Ni_2(Mo,Cr)$ precipitates allowing dislocations to more easily pass through the precipitates in the material given only the first stage of the heat treatment.

5. Conclusions

HAYNES 242 alloy specimens subjected to one- and two-step heat treatments exhibited similar grain sizes, phase compositions and mechanical properties. However, the scale of the ordered $Ni_2(Mo,Cr)$ precipitates differed substantially between the two heat treatments. Molybdenum was found to partition to these lenticular precipitates, whereas nickel, iron, aluminum, silicon and manganese partitioned to the disordered γ matrix. Chromium did not significantly partition between these two phases, but was found to segregate to the interface between the phases. Molybdenum, boron, phosphorous, and carbon exhibited substantial segregation to the grain boundaries.

Acknowledgements

HAYNES is a registered trademark and 242 is a trademark of Haynes International, Inc. The authors would like to thank K.F. Russell for her technical assistance. Research at the Oak Ridge National Laboratory SHaRE User Facility was sponsored by the Laboratory Technology Research Program, through a CRADA with Haynes International, Inc., and by the Division of Materials Sciences and Engineering, U.S. Department of Energy, under contract number DE-AC05-00OR22725 with UT-Battelle, LLC.

References

[1] M.F. Rothman, S.K. Srivastava, World Aerospace Profile, Sterling Publications, London, 1989.
[2] S.K. Srivastava, M.F. Rothman, High Temperature Materials for Power Engineering, Kluwer Academic Publishers, Dordrecht, Netherlands, 1990, pp. 1357–1366.
[3] S.K. Srivastava, in: S.D. Antolovich, R.W. Stusrud, R.A. MacKay, D.L. Anton, T. Khan, R.D. Kissinger, D.L. Klarstrom (Eds.), Superalloys 1992, TMS Publications, Warrendale, PA, 1992, pp. 227–236.
[4] M. Kumar, V.K. Vasudevan, Acta Mater. 44 (1996) 1591–1600.
[5] L.M. Pike, D.L. Klarstrom, I.J. Storey, M.F. Rothman, Parsons 2000: Advanced Materials for 21st Century Turbines and Power Plant, in: A. Strang et al. (Eds.), Institute of Materials Communications, London, 2000, pp. 755–766.
[6] M.K. Miller, Atom Probe Tomography, Kluwer Academic/Plenum Press, New York, NY, 2000.
[7] S.K. Das, G. Thomas, Phys. Stat. Sol. A 21 (1974) 177–190.